Electronic band structure of epitaxial $CuInSe_2$ films

Andreas Hofmann and Christian Pettenkofer*

Helmholtz-Zentrum Berlin, Institute for Charge Carrier Dynamics E-I4, Albert-Einstein-Strasse 15, D-12489 Berlin, Germany

(Received 6 June 2011; published 14 September 2011)

We report on a synchrotron radiation-based angle-resolved photoelectron spectroscopy study of the chalcopyrite semiconductor $CuInSe_2$. Clean and well-ordered samples with surface orientations (001) and (112) were prepared by molecular beam epitaxy on GaAs (100) and (111)A wafers with a miscut, which allows for the growth of single-domain samples. Band dispersions perpendicular (Γ-T) and parallel (Γ-N) to the surface of near-stoichiometric (001) samples show a strikingly good agreement with density functional theory calculation, although a distinct narrowing of the density of states gap around $E_B = 3$ eV is observed. The band structure for the Γ-N direction can also be obtained by in-plane measurements of the (112) surface. The results are consistent with the (001) surface and implications of polarization dependency are discussed.

DOI: 10.1103/PhysRevB.84.115109 PACS number(s): 71.20.−b, 79.60.Bm, 88.40.jn

I. INTRODUCTION

$CuInSe_2$ is the prototype chalcopyrite semiconductor and its alloys with Ga are applied in the most efficient polycrystalline thin-film solar cells available today.[1] In order to push the energy conversion efficiency of devices closer to the theoretical limit, these materials have been studied intensively during the last decades.[2] During this process, some of the unusual physical properties of chalcopyrites, such as the large tolerance to deviations from the ideal stoichiometry, intrinsic doping, and the electrically benign behavior of grain boundaries could be explained.[3] Many of the recent experimental studies aimed at the improvement of devices and therefore polycrystalline absorbers taken from base line processes were widely investigated.

Despite the improvement in experimental methods and accuracy, there are only a few recent works that investigate the fundamental properties of single-crystalline material.[4,5] In particular, this allows for studying the dependency of heterocontact formation and band alignment on the surface exposed to the contact plane.[6,7] On the other hand, theoretical work on the band structure ranges from early semiempirical calculations[8] and the fundamental density functional theory (DFT) work by Jaffe and Zunger[9] to recent refinements of the exchange-correlation functional.[10,11]

The reason for the lack of experimental studies is presumably the difficulty of preparing clean, well-ordered and oriented surfaces that are free of contaminations. Sufficiently large single crystals that allow for a defined cleavage are difficult to obtain, and this method is restricted to (011) planes.[12,13] In contrast, the (001) plane gives access to symmetry directions and is thus interesting for angle-resolved photoemission spectroscopy (ARPES) measurements and in particular the natural growth plane (112) is technologically relevant.

The higher symmetry of the zinc blende-type substrates compared to the chalcopyrite results in different possible orientations of the epilayer and hence domain formation during growth.[14] This can be suppressed by using stepped substrates which induce step-flow growth along step edges.[15]

We prepared epitaxial $CuInSe_2$(001) and (112) films on GaAs wafers in order to study the electronic valence band structure with angle-resolved photoemission. Single-domain epilayers were obtained and results are contrasted with recent DFT calculations. This paper is organized as follows: Sec. II gives an overview about the k-space topology and calculated band structures of chalcopyrites; the experimental details are explained in Sec. III; the subsequent Sec. IV discusses the experimental band structures for the stoichiometric (001) surface; the final Sec. V presents data for the (112) surface.

II. k-SPACE AND ELECTRONIC STRUCTURE

The chalcopyrite crystal structure is derived from the zinc blende lattice which is common to many binary semiconductor compounds. The presence of a second cation species together with a lowering in total energy introduces an ordering of the cation sublattice. Starting from the cubic zinc blende unit cell, the chalcopyrite order doubles the size of the unit cell along the c axis (Fig. 1). As a result of the larger unit cell, the Brillouin zone (BZ) of the tetragonal lattice is shrunken compared to the zinc blende case. Additionally, the anions are bound to two different types of cations which leads to the tetragonal distortion of the unit cell $c \neq 2a$. The influence of the tetragonal distortion on the band structure can be directly observed at the valence band maximum (VBM) at the Γ point of the k space. The originally triply degenerate VBM is energetically split in the states I and II (Ref. 16) (see also Fig. 4). This splitting is roughly proportional to the magnitude of the distortion and weak in $CuInSe_2$ due to a small tetragonal displacement. Additional spin-orbit splitting lifts the degeneracy completely (band III in Fig. 4).

The upper valence band of $CuInSe_2$ is dominated by Cu 3d-Se 4p interactions. This constitutes the main difference between chalcopyrites and its zinc blende-type II-VI counterparts and explains the drastic band-gap reduction ($E_g^{CuInSe_2} = 1.04$ eV, $E_g^{ZnSe} = 2.68$ eV, $E_g^{CdSe} = 1.85$ eV).[17] The energetic proximity of Cu 3d and Se 4p leads to a repulsive interaction and pushes the antibonding component "upwards" in energy and thus reduces the band gap. This p-d repulsion, associated with the presence of nondispersive and unhybridized d electron levels has been discussed in the case of silver halides in detail by Tejeda *et al.*[18] Partial density of states (DOS) measurements by synchrotron-based ultraviolet photoemission spectroscopy

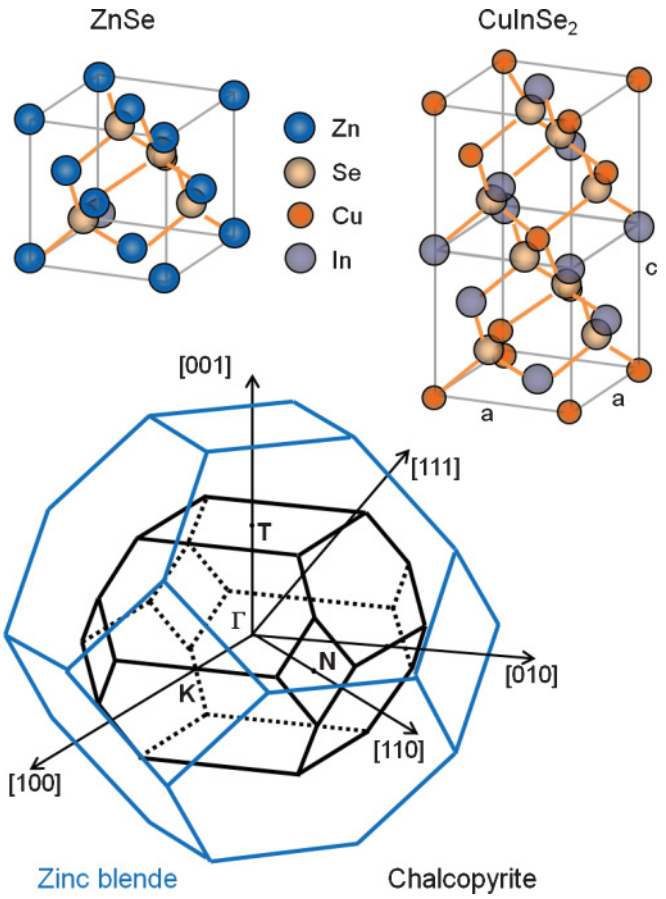

FIG. 1. (Color online) Comparison of the cubic zinc blende and tetragonal chalcopyrite unit cell. The chalcopyrite order of cations doubles the size of the unit cell in the direction of the c axis. Also shown are the corresponding Brillouin zones.

confirmed the energetic overlap of Cu- and Se-derived valence band states.[19]

The $CuInSe_2$ valence band can therefore be structured into the following parts: (1) The dispersive bands of the VBM derived from antibonding Cu-Se states. (2) The nonbonding Cu $3d$ states with nondispersive character at $\sim$2 eV below the VBM and a roughly 1-eV wide DOS gap centered at 2.6 eV. (3) The bonding Cu-Se bands with dominant Se $4p$ character below the gap. (4) The In-Se bands at a binding energy of $\sim$6 eV (see theoretical band structure plots in Figs. 3 and 4). The surface band structure consists mainly of surface resonances in the band gap which exhibit flat dispersion.[20] Therefore, no significant mixing of the surface states with bulk bands has to be expected.

III. EXPERIMENT

$CuInSe_2$ films were prepared from elemental Cu, In, and Se sources by molecular beam epitaxy on $GaAs(100)_{zb}$ (2° miscut towards $[01\text{-}1]_{zb}$) and $(111)A_{zb}$ (5° miscut towards $[100]_{zb}$) substrates with stepped surfaces. The GaAs wafers were wet-chemically etched and sulfur terminated prior to insertion into the ultrahigh vacuum system.[21,22] The sample temperature during growth was $T = 550$ °C and 525 °C for (001) and (112) samples, respectively. Under these conditions, the growth rate was $\sim$5 nm/min and the typical $CuInSe_2$ epilayer thickness was 100 nm. On the $GaAs(100)_{zb}$ substrate, $CuInSe_2$ grows preferentially with a c-axis orientation parallel to the surface normal, as confirmed by reflection high-energy electron diffraction,[23] resulting in a $CuInSe_2(001)$ surface. This is attributed to a minimization of strain energy. Because of the tetragonal distortion, the $CuInSe_2$ c axis exhibits a larger lattice mismatch with the GaAs substrate than the a axis ($c_{CuInSe_2}/2 > a_{CuInSe_2} > a_{GaAs}$). This behavior is beneficial for the angle-resolved photoemission measurements, in that it leads to c-oriented single-domain $CuInSe_2(001)$ samples. Otherwise, contributions from misoriented domains would appear in the spectra. Compared to the (100) surface of a zinc blende lattice, $CuInSe_2(001)$ exhibits a (4×2) reconstruction in low-energy electron diffraction (LEED) images.[24] This surface order is present directly after molecular-beam epitaxy (MBE) growth for substrate temperatures above 500 °C. Despite the lower symmetry of the (4×2) reconstruction compared to the $CuInSe_2(001)$ surface, only a single rotational domain of the reconstruction is observed. Apparently, this order is induced by terrace steps of the substrate.

The chalcopyrite (112) planes which grow on $GaAs(111)_{zb}$ substrates exhibit a twofold and thus lower symmetry than the $GaAs(111)_{zb}$ planes. Therefore, depending on the alignment of the c axis with respect to the substrate, three different

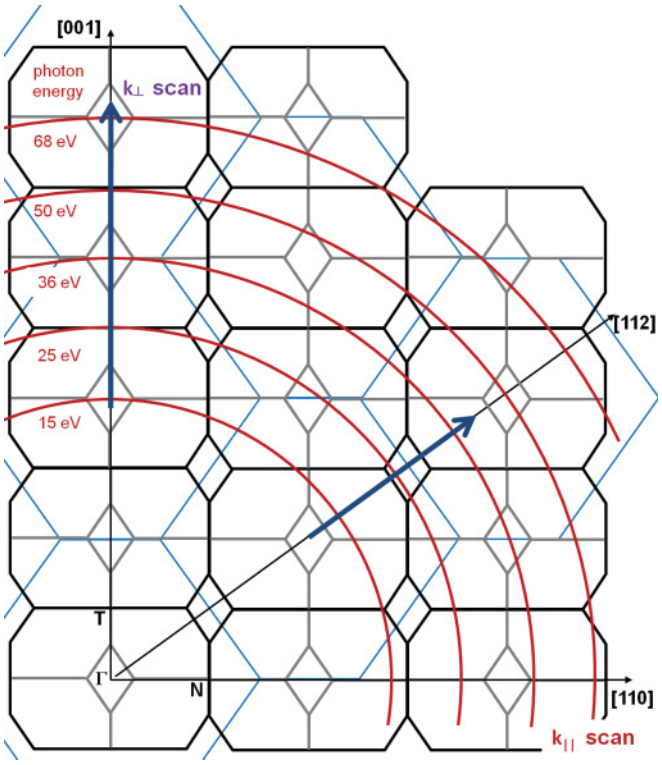

FIG. 2. (Color online) Photoemission paths in reciprocal space for materials with tetragonal (chalcopyrite unit cell, black) and fcc symmetry (zinc blende, blue). Depicted is a cut through the (1-10) plane of the chalcopyrite lattice. The radius of the sphere of photoemission final states (dark red) is related to the photon energy. Paths of $k_\perp$ scans performed in normal emission on (001) and (112) surfaces by variation of the photon energy are indicated by arrows (dark blue).

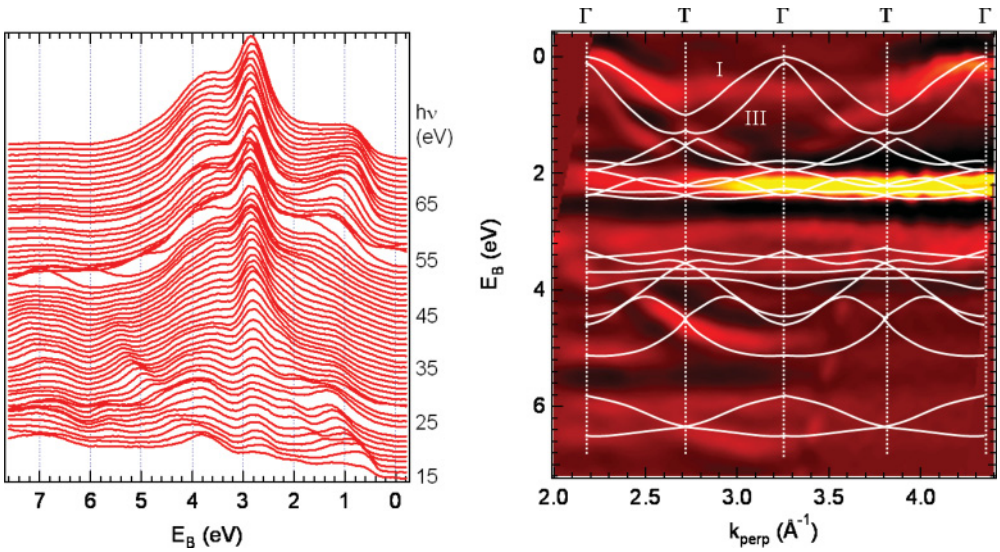

FIG. 3. (Color online) Left: Waterfall plot of normal emission spectra recorded with $h\nu = 15$–72 eV for $CuInSe_2(001)$. A clear dispersion is observed for the VBM. Right: Second derivative image of the $E(k)$ matrix for the $k_\perp$ scan data. The VBM was set to $E_B = 0$. The DFT-LDA calculation in the Γ-T direction by Belhadj *et al.*[10] is superimposed.

orientations of the $CuInSe_2(112)$ epilayer are possible, each rotated by 120° around the surface normal.[25] This is confirmed by the hexagonal LEED pattern with sixfold symmetry obtained for chalcopyrites grown on flat $(111)_{zb}$ substrates. In contrast, the $c(4 \times 2)$ reconstruction of the zinc blende pattern could be obtained for $CuInSe_2(112)$ on the miscut substrate.[26] This corresponds to the chalcopyrite order of cations at the (112) surface[27] and also confirms the presence of only a single chalcopyrite domain.

Stoichiometry and surface order were checked with x-ray photoemission spectroscopy and LEED in our integrated ultrahigh vacuum system connected to the MBE chamber. Subsequently, the $CuInSe_2$ epilayers were capped with a protective selenium layer[28] (>100 nm thick) and transferred to the angle-resolved photoemission system connected to the TGM7 dipole beamline at BESSY II. The Se layer was removed by heating the sample to $T = 300$ °C, which is confirmed by the reappearance of the LEED pattern and the characteristic valence band shape of $CuInSe_2$. The ARPES system is equipped with a Scienta SES-50 electron spectrometer, mounted on a two-axis goniometer in order to vary the measured electron emission angle. The acceptance angle for the parallel detection of electrons in the analyzer is 8° and the angular resolution was set to 0.3°. The photon energy was varied in the range from 10 to 70 eV with an overall energy resolution between ∼100 and 150 meV. All data were collected at room temperature. The surface normal of the sample was rotated by 45° with respect to the incident beam and the polarization vector was parallel to this plane (p polarization). For measurements of the crystal momentum parallel to the surface plane, the spectrometer could be moved either parallel or perpendicular to the polarization vector.

During the photoemission process, energy and momentum conservation holds, which allows for a connection between kinetic energy and takeoff angle of the photoelectron and the probed initial state in the solid.[29] The momentum component parallel to the surface is readily conserved, and can therefore directly be calculated by

$$k_{||} = \frac{\sqrt{2\pi}}{\hbar}\sqrt{E_{\mathrm{kin}}}\sin\vartheta. \tag{1}$$

However, due to the surface potential, the momentum component perpendicular to the surface is not conserved. This effect is accounted for by the inner potential V_0, and with the approximation of free-electron-like final states, the $k_\perp$ value can be related to the kinetic energy:

$$k_\perp = \frac{\sqrt{2\pi}}{\hbar}\sqrt{E_{\mathrm{kin}}\cos^2\vartheta + V_0}. \tag{2}$$

Thus the k-resolved band structure perpendicular to the surface of the sample can directly be obtained by variation of the photon energy for the photoemission spectra. Photoemission paths that are accessed by a variation of the emission angle can be illustrated with a cut through k space, in this case the (1-10) plane (Fig. 2). For constant excitation energy, this path is curved and states for different emission angles correspond to different $k_\perp$ values. Therefore, measurements exactly along symmetry directions in k space are not possible with this method.

IV. $CuInSe_2(001)$

On the contrary, this is possible for $k_\perp$ scan in normal emission. In addition, this method gives an overview of the obtainable band structures and allows for the determination of energies which access symmetry points of the k space. For the (001) surface, the excitation energy was varied from 15 to 24 eV in steps of 0.5 eV and from 24 to 72 eV in steps of 1 eV. According to the schematic in Fig. 2, this energy range comprises a scan from the third to the fifth BZ in $k_\perp$. The corresponding spectra are plotted in Fig. 3. A dispersion of the topmost valence band is clearly observed, while the nonbonding copper states around 3 eV show only

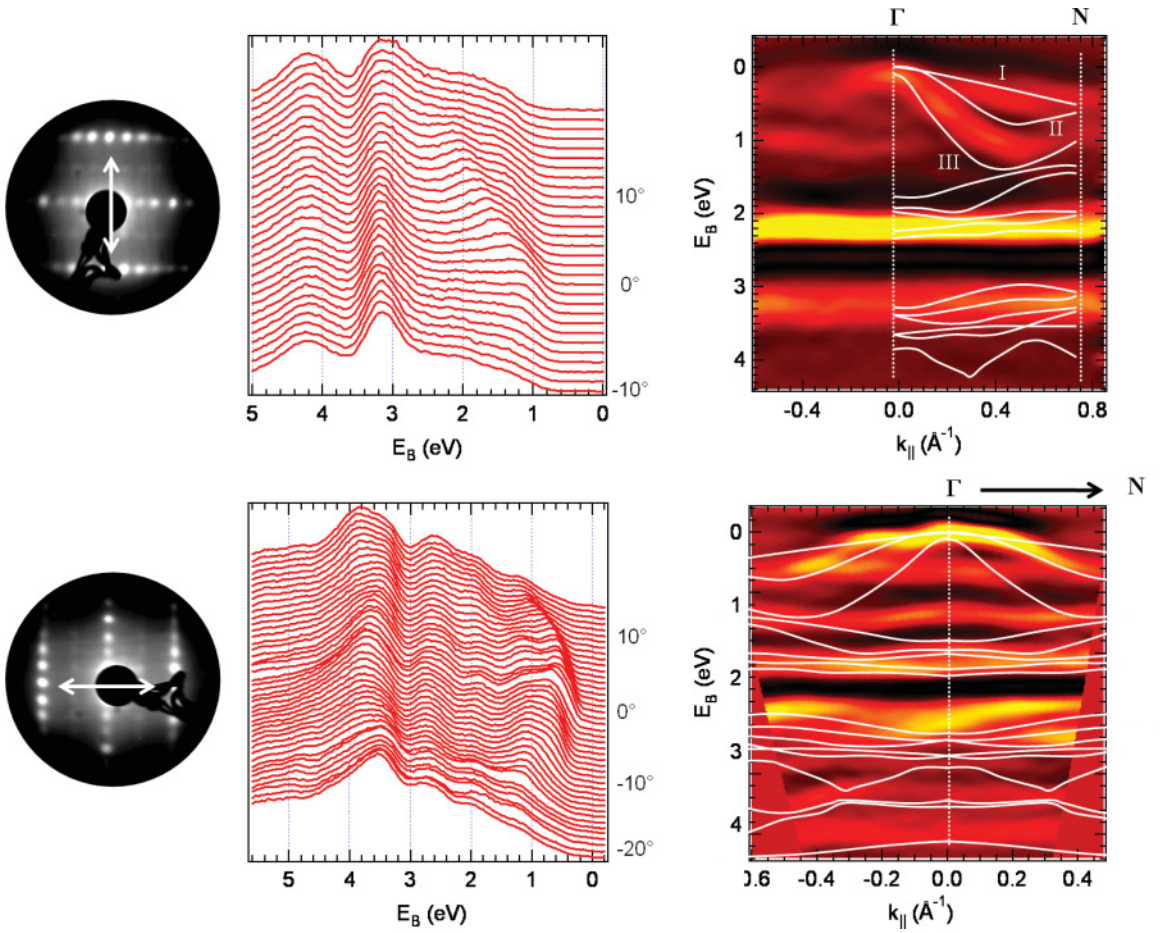

FIG. 4. (Color online) Left: LEED image of the $CuInSe_2(001)$ surface recorded at 58-eV electron energy showing the (4×2) reconstruction with respect to the zinc blende surface BZ. The arrows indicate the $k_{\|}$ scan direction for the respective ARPES spectra. Top: Waterfall plot of the angular spectra for $CuInSe_2(001)$ measured at 60-eV photon energy, which shows a strong dispersion of the VBM. Also shown is the corresponding second derivative $E(k)$ matrix, the DFT calculation for Γ-N (Ref. 10) is superimposed. Bottom: Same for $h\nu = 15$ eV, the scan was performed in the polarization plane.

minor changes in binding energy. The overall shape of the valence band is in good agreement with previous publications on single-crystalline $CuInSe_2$.[19] For a direct comparison with theoretical calculations, the data were converted to an $E(k)$ matrix by employing Eq. (2). In order to derive the inner potential value, the valence band maximum was found for the spectrum recorded at $h\nu = 15$ eV, which was identified with the Γ point of the third Brillouin zone in $k_{\perp}$. This yielded a V_0 of (9.0 ± 1.0) eV. The second derivative in energy of the $E(k)$ matrix was calculated in order to enhance the contrast of prominent features compared to the secondary electron background. This measure narrows the linewidth of photoemission peaks artificially and distorts the relative amplitudes but clarifies the shape of band dispersions and allows for a direct comparison with band structure calculation (Fig. 3).

The overlay with DFT band structure for Γ-T from Ref. 10 proves that all characteristic features of the $CuInSe_2$ valence band are present in the data. The width of the topmost band (I) is reduced compared to the calculation from 1.0 to 0.8 eV, while the width of band (III) appears larger in the experimental data. The nonbonding Cu $3d$ bands are nicely reproduced; the DOS gap between nonbonding Cu $3d$ and bonding Cu $3d$-Se $4p$ bands is also clearly seen; however, the width of the gap is reduced in the experimental data to 0.7 eV. The weak dispersion of states below the DOS gap is again in agreement with the calculation. With the previously extracted inner potential, the Γ points and valence band maxima for the fourth and fifth BZ should be probed for 36- and 68-eV excitation energy, respectively. The corresponding positions in the $E(k)$ plot are marked in Fig. 2. The Γ point is weakly developed for the fourth BZ, but there is good coincidence for low-lying bonding Cu-Se bands between 4- and 5-eV binding energy and the In-Se bands around 6 eV. The suppression of the photoemission intensity near the VBM can be understood in terms of a forbidden transition of the dipole matrix element. For the fifth BZ, a valence band maximum at the Γ point is visible, while the states at higher binding energies are faded, presumably due to a low cross section of mainly Se-derived states. The observed periodicity of structures reflects the BZ symmetry in $k_{\perp}$ and proves the chalcopyrite order of $CuInSe_2$ epilayers.

For such a large variation in excitation energy, two aspects need to be considered: The change in photoionization cross

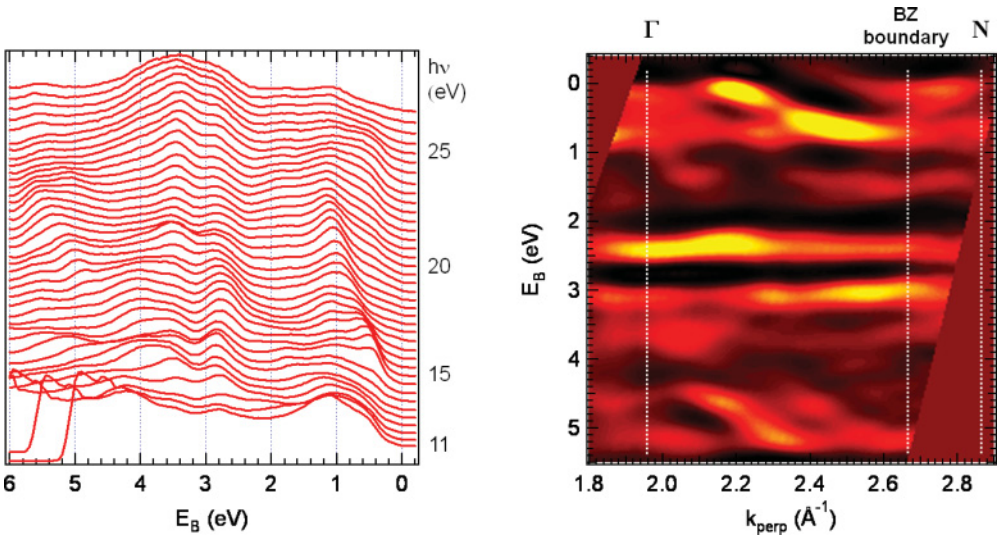

FIG. 5. (Color online) $E(k)$ data for $CuInSe_2(112)$ recorded in normal emission for $h\nu = 11$–28 eV in second derivative representation. Indicated symmetry points of k space were calculated by using the inner potential extracted from the $CuInSe_2(001)$ data.

section (PICS) for the contributing states and inelastic mean free path of the photoelectrons. When the photon energy is increased from 15 to 72 eV, the PICS of the Se 4*p* states is lowered compared to Cu 3*d* states,[30] which is confirmed by the amplification of the nonbonding Cu states compared to the residual valence band features. A reduction of the mean free path enhances surface sensitivity, which becomes maximal for the universal mean free path minimum at $E_{\mathrm{kin}} \approx 50$ eV. Despite the surface sensitivity of the technique, the dispersion in $k_\perp$ spectra that is observed in the data proves the bulk character of electron bands. Surface states are nondispersive due to their two-dimensional character. However, this does not mean that the states above and below the DOS gap, which exhibit a weak dispersion, are surface states. Instead, their lack of energy dispersion is predicted by calculation of the bulk bands, especially by Ref. 11. However, the reduced width of the DOS gap is predicted by neither of the calculations.

Having analyzed the spectra for the Γ-*T* direction from the $k_\perp$ measurement, we now consider the $k_\parallel$ spectra, which give access to the Γ-*N* [110] direction. For the angle-resolved measurements, the sample was aligned with the analyzer slit, which was also the scan direction, by means of the LEED pattern. The scan was performed perpendicular to the polarization plane. Figure 4 shows data recorded at 60-eV excitation energy. This transition does not correspond to the exact position of the Γ point in $k_\perp$, but the intensity near the valence band maximum is strongly faded for larger excitation energies.

The raw data show a strong dispersion on angle variation, which proves again the quality of samples and data and the possibility to observe the valence band structure. The bandwidth of antibonding Cu-Se bands slightly reduces compared to calculation, and the slope of these bands (which corresponds to the effective mass) is not exactly reproduced. This could be explained with the position in $k_\perp$ that differs slightly from the Γ point. In addition, the distance from VBM to Cu 3*d* states is ∼0.2 eV smaller than the DFT-local density approximation (LDA) bands. The states below 4.5 eV are mainly Se 4*p* whose intensity is faded due to low cross section.

Due to the changes in PICS and surface sensitivity with photon energy that were mentioned before, another $k_\parallel$ data set was measured at $h\nu = 15$ eV which corresponds to the third BZ Γ point (Fig. 4). This time, the angular scan was performed perpendicular to the analyzer slit and in the polarization plane. Again, the energetic position of states and the size of the DOS gap coincide nicely with the calculation. A closer inspection of bands at the valence band maximum shows only the middle band (II) clearly while there is only faint indication of the spin-orbit split band (I) at negative k values and the crystal-field split band is absent. On the other hand, additional weakly dispersive states are present between valence band maximum and Cu 3*d* states, which correspond to the states observed in the $k_\perp$ data.

V. $CuInSe_2(112)$

The (112) surface is considered to be the natural growth surface of $CuInSe_2$ (Ref. 31) and hence predominant in the grains in polycrystalline solar cell absorbers. Therefore, high-quality films can be expected. For direction accessed by $k_\perp$ measurements, however, no suitable calculation is available. The $k_\perp$ scan presented in Fig. 5 covers a photon energy range from 11 to 28 eV. The most prominent feature in the raw data is the top valence band, which shows a strong dispersion towards higher binding energies for excitation energies >15 eV. Assuming the same inner potential as for the (001) surface, the Γ point and thus the valence band maximum should be probed with 12-eV photon energy for the (112) surface (see Fig. 2), but apparently, the emission is suppressed at this energy. While the states above and below the DOS gap at 3 eV remain at constant binding energies, another dispersive feature is observed among the bonding Cu-Se states. The data were converted to an $E(k)$ matrix by applying Eq. (2), and again the second derivative is shown for enhanced contrast. Symmetry points of the k space were calculated from the inner

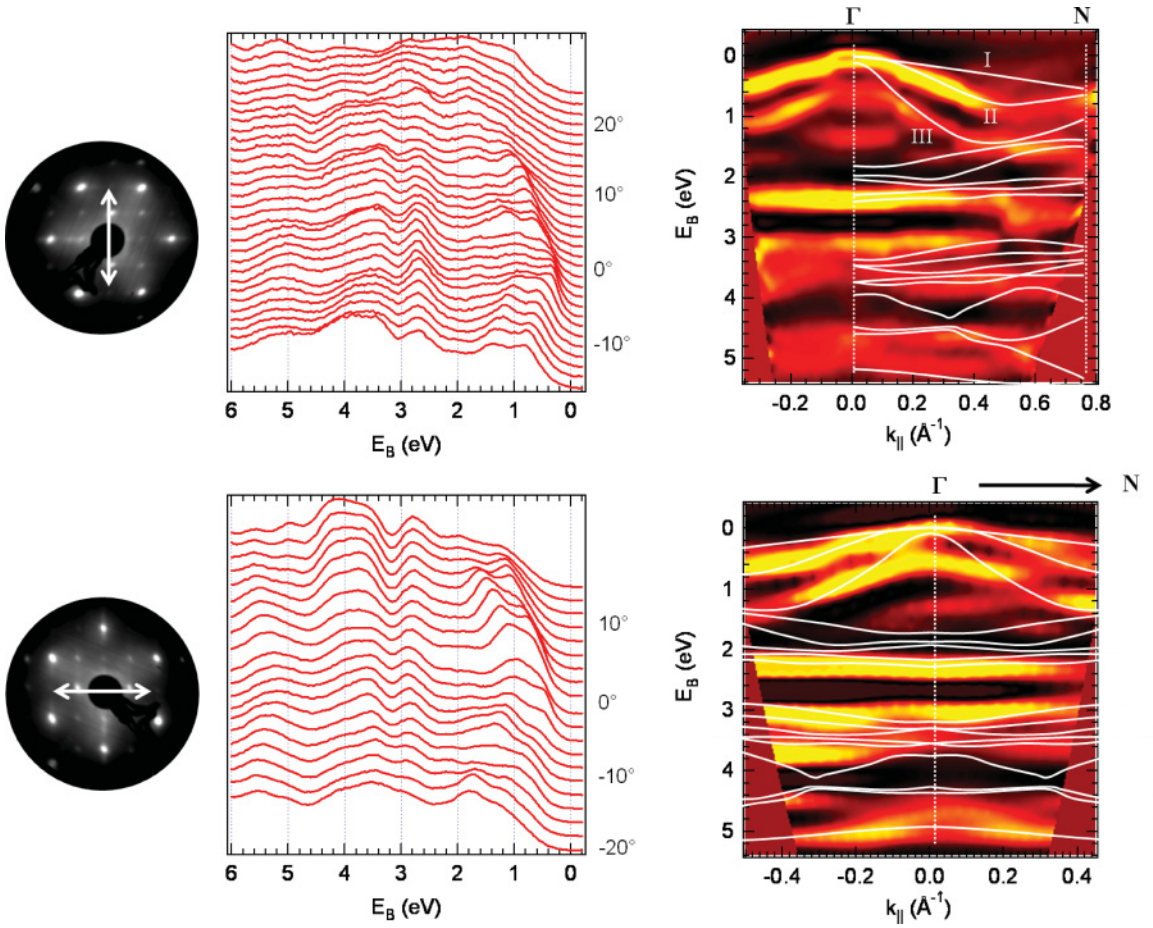

FIG. 6. (Color online) ARPES spectra for $CuInSe_2$(112) recorded at $h\nu = 15$ eV. Top: Data for [1-10] direction recorded perpendicular to the polarization plane. The LEED image (64 eV) for the stoichiometric $CuInSe_2$(112) surface shows the $c(4 \times 2)$ chalcopyrite superstructure. The arrow shows the ARPES scan direction. Also shown is the energy distribution curve waterfall plot for the different emission angles and the second derivative image, together with the DFT bands for Γ-*N* (Ref. 10). Bottom: Same for measurement in the polarization plane.

potential of Sec IV. The width of the strongly dispersive top valence band is 0.8 eV and the DOS gap between second derivative extrema of nondispersive states is 0.7 eV.

The angular scan for $h\nu = 15$ eV excitation energy was performed parallel and perpendicular to the polarization plane. Raw data and $E(k)$ plots are shown in Fig. 6; the scan direction is indicated in the LEED pattern. In both cases, the raw data show a distinct valence band maximum for normal emission which corresponds to the Γ point and clear band dispersion. Comparison of the $E(k)$ matrices with calculation reveals interesting differences: In the perpendicular measurement data along [110], the top valence band (I) is absent, while (II) is excellently reproduced. The energy gap between the spin-orbit split band (III) and the VBM is significantly larger (∼0.4 eV) than in the calculation (0.1 eV) or in the literature [0.19 eV (Ref. 3)]. However, when the *N* point is approached, the coincidence with calculation becomes very good. A rotation of the sample by 90° aligns the Γ-*N* direction in the polarization plane. In this geometry, the band structure exhibits a strong asymmetry around the Γ point. While the left side of the data resembles the perpendicular data that in band (I) is absent, band (II) fits calculations and (III) shows a large spin-orbit splitting and then approaches calculations. On the right side, (I) is present in the data, but the spin-orbit split band now differs strongly from calculations.

In order to access the In-Se states of the lower valence band, another data set recorded at $h\nu = 24$ eV is shown in Fig 7. Fundamental to all angular scan measurements is that different $k_\perp$ positions are probed simultaneously due to the covered binding energy range. According to the free-electron final state model, the valence band maximum is measured near an *N* point in $k_\perp$ by this choice of photon energy. However, a faint maximum is observed, while a minimum is expected. This is indicative of scattering from additional initial states and hence indirect transitions as a result of the $k_\perp$ broadening of the photoelectron final state. The low-lying In-Se bands are probed closer to the Γ point. Both bands are visible and show a nice agreement with calculation. On the other hand, the upward bending of the lowest binding Cu-Se bands is absent in DFT.

VI. DISCUSSION

The photoemission data recorded for epitaxial $CuInSe_2$ films show clear dispersion of valence electron states and in general a convincing agreement with modern band structure calculations. The constituent parts of the valence band can

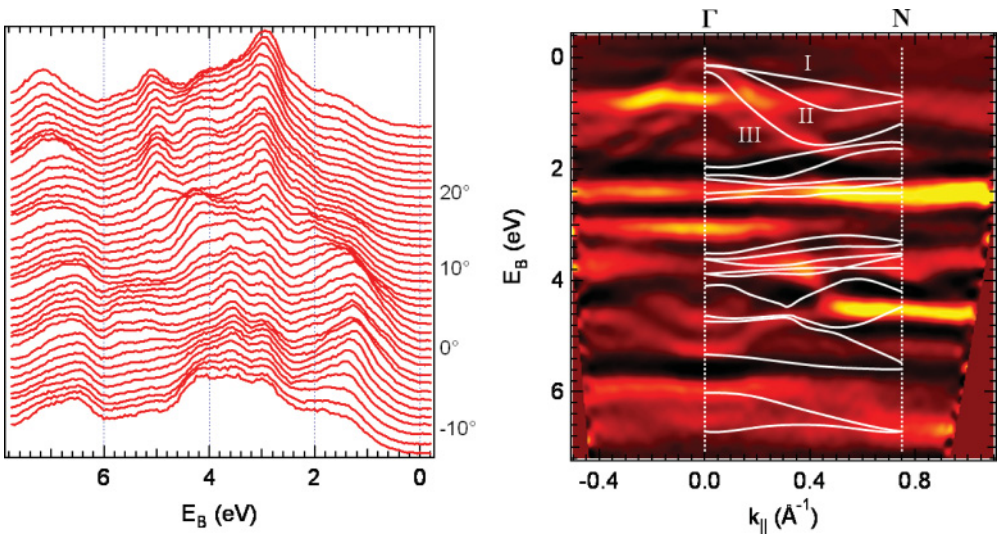

FIG. 7. (Color online) ARPES data for $CuInSe_2$(112) measureed at $h\nu = 24$ eV. The waterfall plot of angular channels is shown together with the second derivative $E(k)$ matrix. The scan was performed perpendicular to the photon polarization plane and parallel to the [1-10] axis.

be distinguished and related to DFT results. However, due to the limitations in resolution and suppression of certain transitions in the photoemission process, a clear assignment between measured and calculated bands is not always possible. The reproducibility of the data is proven by the convincing agreement of our data with the $k_\perp$ measurement for $h\nu = 10$–28 eV on $CuInSe_2$(001) published earlier.[32]

Additional complications that have not been considered so far, but which play a decisive role in photoemission, are the influence of the matrix element and the photoemission final state. Especially for small excitation energies, the photoemission final states may deviate significantly from the free-electron approximation. In that case, the measured photocurrent cannot be simply identified with the initial, i.e., valence band states, and the exact anatomy of the photoemission initial and final states has to be considered.[33,34] The effect of the dipole matrix element is mainly a parity argument, but can be significant when linearly polarized radiation is used as it was done here.

Apart from the early works by Poplavnoi and Polygalov[8] and Jaffe and Zunger,[9] which exhibit significant deviations from experiment, the more recent DFT-LDA (local density approximation) calculations describe our data quite well. The description of semiconductor band structures with DFT-LDA experiences two main problems: the underestimation of the optical band gap and the localization of the *d*-electron bands. Especially the error of the LDA band gap is large and requires the addition of a self-interaction correction or quasiparticle extensions (e.g., GW approximation).[35] In the series from III-V over II-VI to I-III-VI_2 semiconductors, the cation *d*-electron states play an increasingly important role in the formation of the valence band. The position of nonbonding Cu 3*d* states given by band structure calculation is well reproduced in our data—also for different orientations and in-plane and perpendicular measurements. In contrast, the DOS gap below the Cu 3*d* states is reduced in any of our measured spectra to 0.6–0.8 eV which is smaller than any of the calculated values (0.94 eV,[10] 0.91 eV,[36] and 0.87 eV[11]). A disagreement regarding the size of the DOS gap below the Cu 3*d* band between DFT-LDA and ARPES is also observed for $CuInS_2$.[37]

In future experiments, it would be interesting to study the Cu-deficient defect compound $CuIn_3Se_5$ in order to verify the changes in band structure predicted by DFT.[35] This so-called β phase of $CuInSe_2$ is situated next to the buffer layer in $CuIn1-xGa_xSe_2$-based solar cells and is expected to be responsible for some of the beneficial electronic properties of the absorber material.[38]

In summary, we have presented a comprehensive ARPES study on the chalcopyrite $CuInSe_2$ surfaces (001) and (112). $k_\perp$ and $k_\parallel$ spectra were obtained for the stoichiometric (001) and (112) surfaces; all of them exhibited clearly dispersing electron bands, as expected from DFT calculation for the respective *k*-space directions. Yet small deviations regarding the position of the spin-orbit split band near the valence band maximum and the DOS gap that is situated below the nonbonding Cu 3*d* was observed. This gap is reduced in our data by 0.2–0.3 eV compared to recent DFT calculations.

*pettenkofer@helmholtz-berlin.de

[1]M. A. Green, K. Emery, Y. Hishikawa, and W. Warta, Prog. Photovoltaics **18**, 346 (2010).
[2]U. Rau and H. W. Schock, Appl. Phys. A **69**, 131 (1999).
[3]S. Siebentritt, M. Igalson, C. Persson, and S. Lany, Prog. Photovolt.: Res. Appl. **18**, 390 (2010).
[4]M. V. Yakushev, F. Luckert, C. Faugeras, A. V. Karotki, A. V. Mudryi, and R. W. Martin, Appl. Phys. Lett. **97**, 152110 (2010).
[5]R. Hunger, C. Pettenkofer, and R. Scheer, Surf. Sci. **447**, 76 (2001).

[6]A. Hofmann and C. Pettenkofer, Appl. Phys. Lett. **98**, 113503 (2011).
[7]S. Andres, C. Lehmann, and C. Pettenkofer, Thin Solid Films **518**, 1032 (2009).
[8]A. S. Poplavnoi and Y. I. Polygalov, Inorg. Mater. **7**, 1527 (1971).
[9]J. E. Jaffe and A. Zunger, Phys. Rev. B **28**, 5822 (1983).
[10]M. Belhadj, A. Tadjer, B. Abbar, Z. Bousahla, B. Bouhafs, and H. Aourag, Phys. Status Solidi **241**, 2516 (2004).
[11]T. Maeda and T. Wada, Jpn. J. Appl. Phys. **49**, 04DP07 (2010).
[12]M. Sander, W. Jaegermann, and H. J. Lewerenz, J. Phys. Chem. **96**, 782 (1992).
[13]A. Klein, T. Löher, C. Pettenkofer, and W. Jaegermann, J. Appl. Phys. **80**, 5039 (1996).
[14]M. Krejci, A. N. Tiwari, H. Zogg, P. Schwander, H. Heinrich, and G. Kostorz, J. Appl. Phys. **81**, 6100 (1997).
[15]R. Hunger, C. Pettenkofer, and R. Scheer, Surf. Sci. **447**, 76 (2001).
[16]J. L. Shay and J. H. Wernick, *Ternary Chalcopyrite Semiconductors: Growth, Electronic Properties and Applications* (Pergamon Press, Oxford, 1975).
[17]J. E. Jaffe and A. Zunger, Phys. Rev. B **29**, 1882 (1984).
[18]J. Tejeda, N. J. Shevchik, W. Braun, A. Goldmann, and M. Cardona, Phys. Rev. B **12**, 1557 (1975).
[19]T. Löher, A. Klein, C. Pettenkofer, and W. Jaegermann, J. Appl. Phys. **81**, 7806 (1997).
[20]H. Totozintle-Huitl and R. Baquero, J. Phys. Chem. **68**, 1 (2007).
[21]K. S. A. Butcher, R. J. Egan, T. L. Tansley, and D. Alexiev, J. Vac. Sci. Technol. B **14** 152 (1996).
[22]K. Ueno, T. Shimada, K. Saiki, and A. Koma, Appl. Phys. Lett. **56**, 327 (1990).
[23]S. Niki, Y. Makita, A. Yamada, O. Hellman, P. J. Fons, A. Obara, Y. Okada, R. Shioda, H. Oyanagi, T. Kurafuji, S. Chichibu, and H. Nakanishi, J. Cryst. Growth **150**, 1201 (1995).
[24]T. Deniouzou, N. Esser, T. Schulmeyer, and R. Hunger, Appl. Phys. Lett. **88**, 052102 (2006).
[25]J. Cieslak, Th. Hahn, H. Metzner, J. Eberhardt, W. Witthuhn, J. Kräußlich, and F. Wunderlich, Phys. Rev. B **75**, 245306 (2007).
[26]S. B. Zhang and S.-H. Wei, Phys. Rev. B **65**, 081402 (2002).
[27]A. Hofmann and C. Pettenkofer, Ph.D. thesis (unpublished).
[28]R. Hunger, T. Schulmeyer, A. Klein, W. Jaegermann, K. Sakurai, A. Yamada, P. Fons, K. Matsubara, and S. Niki, Surf. Sci. **557**, 263 (2004).
[29]S. Hüfner, *Photoelectron Spectroscopy: Principles and Applications*, Springer Series in Solid-State Science (Springer, Berlin, 1995).
[30]J. J. Yeh and I. Lindau, At. Data Nucl. Data Tables **32**, 2 (1985).
[31]S. Siebentritt, N. Papathanasiou, J. Albert, and M.-C. Lux-Steiner, Appl. Phys. Lett. **88**, 151919 (2006).
[32]R. Hunger and C. Pettenkofer, Mater. Res. Soc. Symp. Proc. **865**, 53 (2005).
[33]X. Y. Cui, E. E. Krasovskii, V. N. Strocov, A. Hofmann, J. Schäfer, R. Claessen, and L. Patthey, Phys. Rev. B **81**, 245118 (2010).
[34]A. L. Walter, J. D. Riley, and O. Rader, New J. Phys. **12**, 013007 (2010).
[35]P. Rinke, A. Qteish, J. Neugebauer, C. Freysoldt, and M. Scheffler, New. J. Phys. **7**, 126 (2005).
[36]S. B. Zhang, S.-H. Wei, A. Zunger, and H. Katayama-Yoshinda, Phys. Rev. B **57**, 9642 (1998).
[37]C. Lehmann, Ph.D. thesis, Brandenburgische Technische Universität, Cottbus, 2007.
[38]D. Schmid, M. Ruckh, F. Grunwald, and H. W. Schock, J. Appl. Phys. **73**, 2902 (1993).